Study of the pion trajectory in the photoproduction of leading neutrons at HERA

ZEUS Collaboration

Abstract

Energetic neutrons produced in ep collisions at HERA have been studied with the ZEUS detector in the photoproduction regime at a mean photon-proton center-of-mass energy of 220 GeV. The neutrons carry a large fraction $0.64 < x_L < 0.925$ of the incoming proton energy, and the four-momentum-transfer squared at the proton-neutron vertex is small, $|t| < 0.425$ GeV^2. The x_L distribution of the neutrons is measured in bins of t. The $(1 - x_L)$ distributions in the t bins studied satisfy a power law $dN/dx_L \propto (1 - x_L)^{a(t)}$, with the powers $a(t)$ following a linear function of t: $a(t) = 0.88 \pm 0.09(\text{stat.})^{+0.34}_{-0.39}(\text{syst.}) - (2.81 \pm 0.42(\text{stat.})^{+1.13}_{-0.62}(\text{syst.}) \text{ GeV}^{-2})t$. This result is consistent with the expectations of pion-exchange models, in which the incoming proton fluctuates to a neutron-pion state, and the electron interacts with the pion.

The ZEUS Collaboration

S. Chekanov, M. Derrick, D. Krakauer, J.H. Loizides[1], S. Magill, S. Miglioranzi[1], B. Musgrave, J. Repond, R. Yoshida
Argonne National Laboratory, Argonne, Illinois 60439-4815, USA [n]

M.C.K. Mattingly
Andrews University, Berrien Springs, Michigan 49104-0380, USA

P. Antonioli, G. Bari, M. Basile, L. Bellagamba, D. Boscherini, A. Bruni, G. Bruni, G. Cara Romeo, L. Cifarelli, F. Cindolo, A. Contin, M. Corradi, S. De Pasquale, P. Giusti, G. Iacobucci, A. Margotti, A. Montanari, R. Nania, F. Palmonari, A. Pesci, G. Sartorelli, A. Zichichi
University and INFN Bologna, Bologna, Italy [e]

G. Aghuzumtsyan, D. Bartsch, I. Brock, S. Goers, H. Hartmann, E. Hilger, P. Irrgang, H.-P. Jakob, O. Kind, U. Meyer, E. Paul[2], J. Rautenberg, R. Renner, A. Stifutkin, J. Tandler[3], K.C. Voss, M. Wang
Physikalisches Institut der Universität Bonn, Bonn, Germany [b]

D.S. Bailey[4], N.H. Brook, J.E. Cole, G.P. Heath, T. Namsoo, S. Robins, M. Wing
H.H. Wills Physics Laboratory, University of Bristol, Bristol, United Kingdom [m]

M. Capua, A. Mastroberardino, M. Schioppa, G. Susinno
Calabria University, Physics Department and INFN, Cosenza, Italy [e]

J.Y. Kim, I.T. Lim, K.J. Ma, M.Y. Pac[5]
Chonnam National University, Kwangju, South Korea [g]

A. Caldwell[6], M. Helbich, X. Liu, B. Mellado, Y. Ning, S. Paganis, Z. Ren, W.B. Schmidke, F. Sciulli
Nevis Laboratories, Columbia University, Irvington on Hudson, New York 10027 [o]

J. Chwastowski, A. Eskreys, J. Figiel, A. Galas, K. Olkiewicz, P. Stopa, L. Zawiejski
Institute of Nuclear Physics, Cracow, Poland [i]

L. Adamczyk, T. Bołd, I. Grabowska-Bołd[7], D. Kisielewska, A.M. Kowal, M. Kowal, J. Łukasik, M. Przybycień, L. Suszycki, D. Szuba, J. Szuba[8]
Faculty of Physics and Nuclear Techniques, AGH-University of Science and Technology, Cracow, Poland [p]

A. Kotański[9], W. Słomiński
Department of Physics, Jagellonian University, Cracow, Poland

V. Adler, U. Behrens, I. Bloch, K. Borras, V. Chiochia, D. Dannheim[10], G. Drews, J. Fourletova, U. Fricke, A. Geiser, P. Göttlicher[11], O. Gutsche, T. Haas, W. Hain, S. Hillert[12], C. Horn, B. Kahle, U. Kötz, H. Kowalski, G. Kramberger, H. Labes, D. Lelas, H. Lim, B. Löhr, R. Mankel, I.-A. Melzer-Pellmann, C.N. Nguyen, D. Notz, A.E. Nuncio-Quiroz, A. Polini, A. Raval, L. Rurua, U. Schneekloth, U. Stösslein, G. Wolf, C. Youngman, W. Zeuner
Deutsches Elektronen-Synchrotron DESY, Hamburg, Germany

S. Schlenstedt
DESY Zeuthen, Zeuthen, Germany

G. Barbagli, E. Gallo, C. Genta, P. G. Pelfer
University and INFN, Florence, Italy [e]

A. Bamberger, A. Benen, F. Karstens, D. Dobur, N.N. Vlasov
Fakultät für Physik der Universität Freiburg i.Br., Freiburg i.Br., Germany [b]

M. Bell, P.J. Bussey, A.T. Doyle, J. Ferrando, J. Hamilton, S. Hanlon, D.H. Saxon, I.O. Skillicorn
Department of Physics and Astronomy, University of Glasgow, Glasgow, United Kingdom [m]

I. Gialas
Department of Engineering in Management and Finance, Univ. of Aegean, Greece

T. Carli, T. Gosau, U. Holm, N. Krumnack, E. Lohrmann, M. Milite, H. Salehi, P. Schleper, T. Schörner-Sadenius, S. Stonjek[12], K. Wichmann, K. Wick, A. Ziegler, Ar. Ziegler
Hamburg University, Institute of Exp. Physics, Hamburg, Germany [b]

C. Collins-Tooth, C. Foudas, R. Gonçalo[13], K.R. Long, A.D. Tapper
Imperial College London, High Energy Nuclear Physics Group, London, United Kingdom [m]

P. Cloth, D. Filges
Forschungszentrum Jülich, Institut für Kernphysik, Jülich, Germany

M. Kataoka[14], K. Nagano, K. Tokushuku[15], S. Yamada, Y. Yamazaki
Institute of Particle and Nuclear Studies, KEK, Tsukuba, Japan [f]

A.N. Barakbaev, E.G. Boos, N.S. Pokrovskiy, B.O. Zhautykov
Institute of Physics and Technology of Ministry of Education and Science of Kazakhstan, Almaty, Kazakhstan

D. Son
Kyungpook National University, Center for High Energy Physics, Daegu, South Korea [g]

K. Piotrzkowski
Institut de Physique Nucléaire, Université Catholique de Louvain, Louvain-la-Neuve, Belgium

F. Barreiro, C. Glasman[16], O. González, L. Labarga, J. del Peso, E. Tassi, J. Terrón, M. Zambrana
Departamento de Física Teórica, Universidad Autónoma de Madrid, Madrid, Spain [l]

M. Barbi, F. Corriveau, S. Gliga, J. Lainesse, S. Padhi, D.G. Stairs, R. Walsh
Department of Physics, McGill University, Montréal, Québec, Canada H3A 2T8 [a]

T. Tsurugai
Meiji Gakuin University, Faculty of General Education, Yokohama, Japan [f]

A. Antonov, P. Danilov, B.A. Dolgoshein, D. Gladkov, V. Sosnovtsev, S. Suchkov
Moscow Engineering Physics Institute, Moscow, Russia [j]

R.K. Dementiev, P.F. Ermolov, I.I. Katkov, L.A. Khein, I.A. Korzhavina, V.A. Kuzmin, B.B. Levchenko, O.Yu. Lukina, A.S. Proskuryakov, L.M. Shcheglova, S.A. Zotkin
Moscow State University, Institute of Nuclear Physics, Moscow, Russia [k]

N. Coppola, S. Grijpink, E. Koffeman, P. Kooijman, E. Maddox, A. Pellegrino, S. Schagen, H. Tiecke, M. Vázquez, L. Wiggers, E. de Wolf
NIKHEF and University of Amsterdam, Amsterdam, Netherlands [h]

N. Brümmer, B. Bylsma, L.S. Durkin, T.Y. Ling
Physics Department, Ohio State University, Columbus, Ohio 43210 [n]

A.M. Cooper-Sarkar, A. Cottrell, R.C.E. Devenish, B. Foster, G. Grzelak, C. Gwenlan[17], T. Kohno, S. Patel, P.B. Straub, R. Walczak
Department of Physics, University of Oxford, Oxford United Kingdom [m]

A. Bertolin, R. Brugnera, R. Carlin, F. Dal Corso, S. Dusini, A. Garfagnini, S. Limentani, A. Longhin, A. Parenti, M. Posocco, L. Stanco, M. Turcato
Dipartimento di Fisica dell' Università and INFN, Padova, Italy [e]

E.A. Heaphy, F. Metlica, B.Y. Oh, J.J. Whitmore[18]
Department of Physics, Pennsylvania State University, University Park, Pennsylvania 16802 [o]

Y. Iga
Polytechnic University, Sagamihara, Japan [f]

G. D'Agostini, G. Marini, A. Nigro
Dipartimento di Fisica, Università 'La Sapienza' and INFN, Rome, Italy [e]

C. Cormack[19], J.C. Hart, N.A. McCubbin
Rutherford Appleton Laboratory, Chilton, Didcot, Oxon, United Kingdom [m]

C. Heusch
University of California, Santa Cruz, California 95064, USA [n]

I.H. Park
Department of Physics, Ewha Womans University, Seoul, Korea

N. Pavel
Fachbereich Physik der Universität-Gesamthochschule Siegen, Germany

H. Abramowicz, A. Gabareen, S. Kananov, A. Kreisel, A. Levy
Raymond and Beverly Sackler Faculty of Exact Sciences, School of Physics, Tel-Aviv University, Tel-Aviv, Israel [d]

M. Kuze
Department of Physics, Tokyo Institute of Technology, Tokyo, Japan [f]

T. Fusayasu, S. Kagawa, T. Tawara, T. Yamashita
Department of Physics, University of Tokyo, Tokyo, Japan [f]

R. Hamatsu, T. Hirose[2], M. Inuzuka, H. Kaji, S. Kitamura[20], K. Matsuzawa
Tokyo Metropolitan University, Department of Physics, Tokyo, Japan [f]

M. Costa, M.I. Ferrero, V. Monaco, R. Sacchi, A. Solano
Università di Torino and INFN, Torino, Italy [e]

M. Arneodo, M. Ruspa
Università del Piemonte Orientale, Novara, and INFN, Torino, Italy [e]

T. Koop, J.F. Martin, A. Mirea
Department of Physics, University of Toronto, Toronto, Ontario, Canada M5S 1A7 [a]

J.M. Butterworth[21], R. Hall-Wilton, T.W. Jones, M.S. Lightwood, M.R. Sutton[4], C. Targett-Adams
Physics and Astronomy Department, University College London, London, United Kingdom [m]

J. Ciborowski[22], R. Ciesielski[23], P. Łużniak[24], R.J. Nowak, J.M. Pawlak, J. Sztuk[25], T. Tymieniecka, A. Ukleja, J. Ukleja[26], A.F. Żarnecki
Warsaw University, Institute of Experimental Physics, Warsaw, Poland [q]

M. Adamus, P. Plucinski
Institute for Nuclear Studies, Warsaw, Poland [q]

Y. Eisenberg, D. Hochman, U. Karshon M. Riveline
Department of Particle Physics, Weizmann Institute, Rehovot, Israel [c]

A. Everett, L.K. Gladilin[27], D. Kçira, S. Lammers, L. Li, D.D. Reeder, M. Rosin, P. Ryan, A.A. Savin, W.H. Smith

Department of Physics, University of Wisconsin, Madison, Wisconsin 53706, USA [n]

A. Deshpande, S. Dhawan

Department of Physics, Yale University, New Haven, Connecticut 06520-8121, USA [n]

S. Bhadra, C.D. Catterall, S. Fourletov, G. Hartner, S. Menary, M. Soares, J. Standage

Department of Physics, York University, Ontario, Canada M3J 1P3 [a]

1   Introduction

Several studies of leading neutron production in ep interactions at HERA have been reported previously [1–5]. Many features of the data are described by pion exchange models, in which the incoming proton fluctuates into a neutron-pion state and the pion interacts with the incoming electron or positron. The kinematic variables t, the square of the four-momentum transfer at the proton-neutron vertex, and x_L, the energy fraction of the proton carried by the neutron, are convenient variables for studying energy-angle correlations. In this study of semi-inclusive photoproduction, $\gamma p \to nX$, where the photon is quasi-real, the energy distribution of leading neutrons is measured as a function of t, which is determined using a new position detector to measure the angle of the neutron. The $(1 - x_L)$ distribution is presented as a function of t for large x_L ($0.64 < x_L < 0.925$) and small $|t|$ ($|t| < 0.425$ GeV^2). The results are interpreted in the context of pion exchange, in order to provide a test of the consistency of this picture of leading neutron production.

2   Experimental set-up and kinematics

The data used for this measurement were collected in the year 2000 at the ep collider HERA with the ZEUS detector, during a short run period in which a special trigger was implemented. The data set corresponds to an integrated luminosity of 9 pb^{-1}. During this period HERA collided 27.5 GeV positrons with 920 GeV protons at a center-of-mass energy of 318 GeV.

Charged particles are tracked in the central tracking detector [6], which operates in a magnetic field of 1.43 T provided by a thin superconducting solenoid and covers the polar-angle[1] region $15° < \theta < 164°$. Outside the solenoid is a hermetic, high-resolution uranium–scintillator calorimeter (CAL) [7] used to measure the energies of the final-state particles.

Bremsstrahlung $ep \to e\gamma p$ and the photoproduction of hadrons $ep \to eX$ are tagged using the luminosity (LUMI) detectors [8]. The bremsstrahlung photons are measured with a lead-scintillator calorimeter located 107 m from the interaction point in the positron-beam direction. A similar calorimeter at 35 m from the interaction point is used to measure positrons scattered at very small angles in an energy range 5-20 GeV, with an energy resolution of $0.19\sqrt{E}$ (E in GeV).

---

[1] The ZEUS coordinate system is a right-handed Cartesian system, with the Z axis pointing in the proton beam direction, referred to as the "forward direction", and the X axis pointing left towards the center of HERA. The coordinate origin is at the nominal interaction point.

ZEUS has two detectors for measuring forward particles, a leading proton spectrometer (LPS) [9], consisting of six stations of silicon strip detectors, and a forward neutron calorimeter (FNC) [10–12] downstream from the LPS, 105 m from the interaction point. The FNC is a lead-scintillator sampling calorimeter, the front section of which is divided into 14 towers, as illustrated in Fig. 1. The hadronic energy resolution, as measured in a pion test beam at 120 GeV, is $0.65\sqrt{E}$ (E in GeV). Three planes of veto counters, located 70, 78, and 199 cm in front of the calorimeter, are used to detect charged particles produced by neutrons interacting in inactive material in front of the FNC.

Magnet apertures limit the FNC geometric acceptance to neutrons inside the area outlined in Fig. 1. This limit corresponds to neutron production angles less than 0.8 mrad; i.e., to transverse momenta $p_T = E_n\theta_n \leq 0.74x_L$ GeV. The neutron production angle, θ_n, is measured with respect to the proton beam direction at the interaction point. The mean value of p_T of the detected neutrons is 0.22 GeV. The overall acceptance of the FNC is about 25% for neutrons with energy $x_L > 0.6$ and $\theta_n < 0.8$ mrad.

The forward neutron tracker (FNT), designed to measure the position of neutron showers, was installed in the FNC in 1998. It consists of two hodoscope planes of 1.2 cm-wide scintillator strips, with 17 strips measuring the X position and 15 strips measuring the Y position. Figure 1 shows the position of the FNT hodoscope in the FNC in the plane transverse to the beam as well as the zero-degree point, the projection of the proton beam direction at the interaction point onto the FNT. The FNT is situated approximately one interaction length inside the FNC. This position is deep enough that a large fraction of the neutrons begin to shower in front of the FNT, but not so deep as to compromise the position resolution. The position resolution of neutron showers in the FNT was measured to be 0.23 cm by placing an adjustable collimator in front of the FNC during special test and calibration runs.

The kinematics of inclusive photoproduction $ep \rightarrow e\gamma p \rightarrow eX$ at HERA is specified by W, the photon-proton center-of-mass energy. This is related to the positron-proton center-of-mass energy, $\sqrt{s}$, by $W^2 = ys$. The inelasticity, y, of the scattered positron is defined by $y = (E - E')/E$, where E (E') is the energy of the incoming (scattered) positron.

To describe the neutron-tagged process $ep \rightarrow e\gamma p \rightarrow enX$, the variables x_L and p_T are also used. These are related to t by

$$t \approx -\frac{p_T^2}{x_L} - \frac{(1 - x_L)}{x_L}\left(m_n^2 - x_L m_p^2\right),$$

where m_p is the mass of the proton and m_n is the mass of the neutron.

3   Event selection

The data sample was collected using a trigger that required at least 5 GeV in the LUMI electron calorimeter in coincidence with at least 0.5 GeV in the rear part ($\theta > 127°$) of the CAL. In addition, the trigger required an energy deposit in the FNC corresponding to $x_L > 0.2$. The trigger efficiency of the FNC was close to 100% for the x_L range under consideration in this paper ($x_L > 0.64$).

Photoproduction events were selected offline using cuts based on the reconstructed vertex position and calorimeter energy deposits. The events were required to have an energy in the LUMI electron calorimeter in the range $10 < E' < 18$ GeV and an energy in the LUMI photon calorimeter smaller than 1 GeV to eliminate bremsstrahlung overlap events. These cuts restricted the photon virtuality, Q^2, to values smaller than ~ 0.02 GeV^2, with a median value of $\approx 10^{-3}$ GeV^2, and resulted in a mean value for W of 220 GeV.

Events with a leading neutron were selected offline by requiring $x_L > 0.64$ and by imposing the following cleaning cuts. Scattered protons, bent into the top towers 11 to 14 of the FNC (Fig. 1) by the HERA dipole magnets, were eliminated by requiring that the tower with the maximum energy deposit be in the range 6 to 9. Photons were removed by eliminating showers with a small energy-weighted vertical width.

Neutrons that started showering in front of the FNC were removed by requiring that the scintillator veto counter farthest from the FNC had an energy deposit below that of a minimum-ionizing particle. To minimize false vetoes due to calorimeter albedo, only the farthest counter was used.

Finally, only events with $x_L < 0.925$ were used in the analysis, since the effect of any error in the energy scale, and the influence of exchanges other than the pion, become significant at high x_L (see Sections 5 and 6, respectively). After these selection cuts, the data sample consisted of 31 756 events.

Not all neutrons start to shower in front of the FNT. To select events with useful position information, it was required that the energy deposited in each plane of the FNT be well above pedestal and that the strips with the two largest energy deposits be adjacent. These cuts reduced the sample to 17 919 events.

4   Neutron efficiencies and correction factors

The efficiencies and correction factors for the leading neutron were calculated with a single-particle Monte Carlo (MC) simulation. The MC program included the geometry of the proton beam-line magnets which define the geometric acceptance, the details of the

absorbing material as obtained from survey measurements, the proton beam divergence, and the measured energy (FNC) and position (FNT) resolutions for hadronic showers. The MC program accounts for the different amount of absorbing material in front of the FNC for the two cases when the ZEUS LPS was, or was not, in the data-taking position. Events were generated using the observed x_L spectrum and an exponential distribution in transverse momentum, $e^{-b(x_L)p_T^2}$. The slope $b(x_L)$ was iterated until the MC distributions matched the observed uncorrected distributions. The corrected data distributions were obtained using bin-by-bin unfolding. The two samples of data, corresponding to the two cases when the LPS was, or was not, in the data-taking position, were corrected independently.

The simulation of the absorbing material was cross-checked by producing a material map from an analysis of low-energy ($x_L < 0.27$) neutron data, under the assumption that low x_L neutrons are distributed uniformly over the geometric acceptance. This assumption is based on noting that both the maximum p_T accepted by the FNC as well as the slope b decrease with x_L [3], and hence the geometric acceptance covers a small region of a slowly changing p_T distribution. An analysis using this material map gives results consistent with those obtained using the material measurements from the survey.

The proton beam had a transverse momentum spread of approximately 0.04 GeV horizontally and 0.1 GeV vertically, as measured by the LPS. The variation of the proton beam orbit was considerably smaller than this spread. The spread broadens the observed position distribution of the neutrons in the FNC, but does not change the peak position.

5   Results

The events were binned in x_L and t. The bins were chosen to be well within the acceptance in the x_L-t plane and contained $12\,523$ events. The corrected x_L distributions of leading neutrons as a function of t are shown in Fig. 2. The distributions are consistent with a power-law dependence in $(1 - x_L)$ of the form $dN/dx_L \propto (1 - x_L)^{a(t)}$. For each t bin the power $a(t)$ was obtained by a least-squares fit of this function to the observed distribution. Only statistical errors were used in the fits because the systematic uncertainties are highly correlated. The resulting fits are superposed on the measured data points.

There are two main sources of systematic uncertainty: an uncertainty of $\pm 2\%$ in the absolute energy scale of the FNC resulting from the calibration procedure [3, 12, 13], and an uncertainty of ± 0.2 cm in each of the X and Y coordinates of the zero-degree point determined from the peak in the X, Y distribution in the FNT [14]. The systematic uncertainties on $a(t)$ were obtained by varying the energy scale and beam-spot position within

their uncertainties and then repeating the complete analysis. The dominant contribution comes from the energy-scale uncertainty.

The powers determined from the fits to the data in Fig. 2 are plotted as a function of $-t$ in Fig. 3. They are consistent with a linear function,

$$a(t) = 0.88 \pm 0.09(\text{stat.})^{+0.34}_{-0.39}(\text{syst.}) - (2.81 \pm 0.42(\text{stat.})^{+1.13}_{-0.62}(\text{syst.})\ \text{GeV}^{-2})t.$$

The correlation between the slope and the intercept is predominantly statistical; the coefficient of correlation is -0.9.

6 Discussion

Previous experiments ([3] and references therein) have shown that leading neutron production in lepton-hadron and hadron-hadron experiments can be described by pion-exchange models. The consistency of this description can be tested by assuming that pion exchange is the dominant mechanism and deriving the pion Regge trajectory from the measured values of $a(t)$.

The pion "flux", the splitting function of a proton to a neutron and pion $(p \rightarrow n\pi^+)$, can be written [15] as

$$f_{\pi/p}(x_L, t) = \frac{1}{4\pi} \frac{g^2_{n\pi p}}{4\pi} \frac{-t}{(m_\pi^2 - t)^2} (1 - x_L)^{1 - 2\alpha_\pi(t)} \left(F(x_L, t)\right)^2, \tag{1}$$

where $g_{n\pi p}$ is the coupling at the $n\pi p$ vertex, m_π is the mass of the pion, and $\alpha_\pi(t) = \alpha'_\pi(t - m_\pi^2)$ is the Regge trajectory of the pion [16]. The function $F(x_L, t)$ is a form-factor which accounts for the effect of hadronic structure on the $p \rightarrow \pi n$ amplitude and for final-state rescattering of the neutron. As discussed elsewhere [2], this prescription for the flux with $F(x_L, t)$ set to 1 describes most of the $pn \rightarrow Xp$ data and also gives a good description of the ZEUS x_L spectrum for photoproduced neutrons [2,3]. In this analysis it is assumed that $F(x_L, t)$ is a function of t only.

The flux is thus of the form $f_{\pi/p} = A(t)\ (1 - x_L)^{1 - 2\alpha_\pi(t)}$. The cross section for neutron production is given by the product of the flux and the total $\gamma\pi$ cross-section $\sigma_{\gamma\pi}(s') = \sigma_{\gamma\pi}\left((1 - x_L)W^2\right)$ as

$$\frac{d^2\sigma}{dx_L dt} = A(t)(1 - x_L)^{1 - 2\alpha_\pi(t)} \sigma_{\gamma\pi}\left((1 - x_L)W^2\right),$$

where $s' = (1 - x_L)W^2$ is the square of the $\gamma\pi$ center-of-mass energy. The total $\gamma\pi$ cross section is assumed to have a power law dependence on s', for large s', of the Donnachie-Landshoff form [17]

$$\sigma_{\gamma\pi}(s') = \mathcal{A}(s')^\epsilon + \mathcal{B}(s')^{-\eta},$$

5

where $\epsilon \approx 0.1$ and $\eta \approx 0.5$. The two terms correspond to the exchange of the Pomeron ($I\!P$) and the Reggeon ($I\!R$), respectively. For large s' the Pomeron contribution dominates that of the Reggeon. In this case the $(1 - x_L)$ distribution is proportional to $(1 - x_L)^{a(t)}$, where

$$a(t) = 1 + \epsilon - 2\alpha'_\pi t.$$

Here m_π^2 has been ignored, since its effect on the result is much smaller than the systematic error. Therefore, the measured linear function $a(t)$ discussed in Section 5 has an intercept of $\alpha_{I\!P}(0) = (1 + \epsilon)$, the value of the Pomeron trajectory at $t = 0$, and a slope of $2\alpha'_\pi$, twice the slope of the pion trajectory.

It is assumed that the $I\!P$ term dominates in the x_L region of this measurement. The fit [17] to the total γp cross section suggests that the highest contribution of the $I\!R$ term is about 12% at $x_L = 0.925$. As x_L decreases (s' increases), the Reggeon contribution falls rapidly. No correction for the Reggeon contribution is applied in this analysis.

Previous measurements of the effective Regge trajectory in the $p \rightarrow n$ transition in hadronic interactions [16, 18, 19] found it to be dominated by the pion, with the intercept in the range -0.1 to 0.3 and the slope in the range 1.1 to 1.3 GeV^{-2}.

The values extracted from the experimental results,

$$1 + \epsilon = \alpha_{I\!P}(0) = 0.88 \pm 0.09 \text{(stat.)}^{+0.34}_{-0.39} \text{(syst.)}$$

and

$$\alpha'_\pi = 1.40 \pm 0.21 \text{(stat.)}^{+0.56}_{-0.31} \text{(syst.)} \text{ GeV}^{-2},$$

are consistent with the expectation that $\alpha_{I\!P}(0)$ is about 1.1 and α'_π is about 1 GeV^{-2} in the range of $0.08 < -t < 0.425$ GeV^2, and so support the hypothesis that pion exchange is the dominant process in this reaction. Note that the data rule out a significant role for ρ exchange. If the ρ trajectory, $\alpha_\rho = 0.5 + t$ [20], is substituted for the pion trajectory in Eq. (1), the value for $1 + \epsilon$ extracted from the data is 1.88 rather than 0.88, which is an inconsistent result for $\alpha_{I\!P}(0)$.

7 Summary

The dependence of the energy distribution of photoproduced leading neutrons on the momentum transfer at the proton-neutron vertex has been studied at an average photon-proton center-of-mass energy of 220 GeV. The $(1 - x_L)$ distributions in bins of t are described by a power law, $dN/dx_L \propto (1 - x_L)^{a(t)}$, with the powers $a(t)$ following a linear function of t: $a(t) = 0.88 \pm 0.09 \text{(stat.)}^{+0.34}_{-0.39} \text{(syst.)} - (2.81 \pm 0.42 \text{(stat.)}^{+1.13}_{-0.62} \text{(syst.)} \text{ GeV}^{-2})t$.

The linear function can be interpreted in the framework of Regge theory. The measured values of the intercept and slope are in agreement with the expectations from pion exchange: i.e., the intercept is the value of the Pomeron trajectory at $t = 0$, and the slope is twice the slope of the pion trajectory. The data thus confirm that the production of leading neutrons in photon-proton collisions is well described by the pion-exchange model.

Acknowledgments

References

[1] ZEUS Coll., M. Derrick et al., Phys. Lett. **B 384**, 388 (1995).

[2] ZEUS Coll., J. Breitweg et al., Nucl. Phys. **B 596**, 3 (2001).

[3] ZEUS Coll., S. Chekanov et al., Nucl. Phys. **B 637**, 3 (2002).

[4] ZEUS Coll., S. Chekanov et al., Phys. Lett. **B 590**, 143 (2004).

[5] H1 Coll., C. Adloff et al., Eur. Phys. J. **C 6**, 587 (1999).

[6] N. Harnew et al., Nucl. Inst. Meth. **A 279**, 290 (1989);
    B. Foster et al., Nucl. Phys. Proc. Suppl. **B 32**, 181 (1993);
    B. Foster et al., Nucl. Inst. Meth. **A 338**, 254 (1994).

[7] M. Derrick et al., Nucl. Inst. Meth. **A 309**, 77 (1991);
    A. Andresen et al., Nucl. Inst. Meth. **A 309**, 101 (1991);
    A. Caldwell et al., Nucl. Inst. Meth. **A 321**, 356 (1992);
    A. Bernstein et al., Nucl. Inst. Meth. **A 336**, 23 (1993).

[8] J. Andruszków et al., Preprint DESY-92-066, DESY, 1992;
    ZEUS Coll., M. Derrick et al., Z. Phys. **C 63**, 391 (1994);
    J. Andruszków et al., Acta Phys. Pol. **B 32**, 2025 (2001).

[9] ZEUS Coll., M. Derrick et al., Z. Phys. **C 73**, 253 (1997).

[10] S. Bhadra et al., Nucl. Inst. Meth. **A 354**, 479 (1995).

[11] S. Bhadra et al., Nucl. Inst. Meth. **A 394**, 121 (1997).

[12] S. Bhadra et al., *Proc. of the Seventh International Conference on calorimetry in High Energy Physics, Tuscon, Arizona, November 1997*, E. Cheu et al. (ed.), p. 295. World Scientific, Singapore (1998).

[13] C.-P. Fagerstroem. Ph.D. Thesis, University of Toronto (1999) (unpublished).

[14] T. Koop. Ph.D. Thesis, University of Toronto (2004) (unpublished).

[15] M. Bishari, Phys. Lett. **B 38**, 510 (1972).

[16] H. Abramowicz et al., Nucl. Phys. **B166**, 62 (1980).

[17] A. Donnachie and P. V. Landshoff, Phys. Lett. **B 296**, 227 (1992).

[18] J. Hanlon et al., Phys. Rev. **D20**, 2135 (1979).

[19] W. Flauger and F. Mönnig, Nucl. Phys. **B109**, 347 (1976).

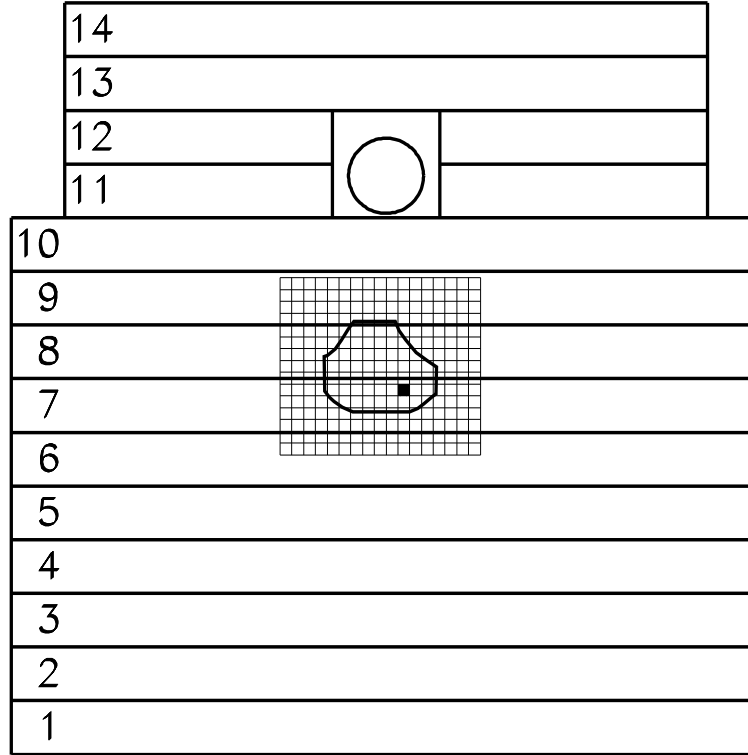[20] R. J. Eden, Rep. Prog. Phys. **34**, 995 (1971).

Figure 1: *The FNC as viewed from the rear with the tower numbers indicated on the left-hand side. The scintillator strips of the FNT hodoscope are shown superposed on towers 6-9 of the FNC. The irregular contour shows the outline of the geometric acceptance allowed by the proton beam-line elements. The full square indicates the approximate position of the projection of the zero-degree line. The proton beampipe, shown as a circle, passes through a hole in the upper part of the FNC.*
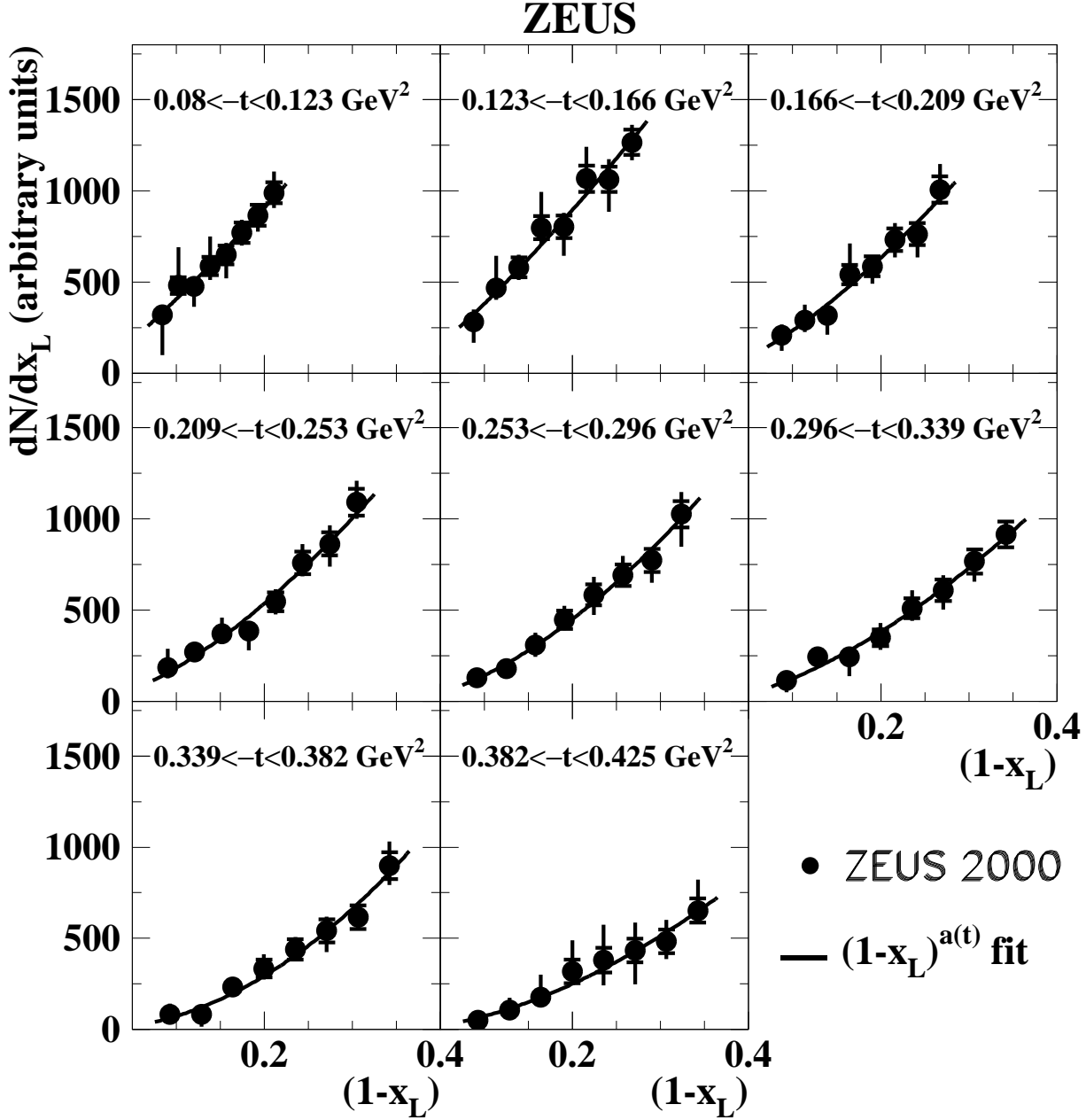
Figure 2: *The x_L distribution in bins of t. The curves show the results of fits to the data with $0.64 < x_L < 0.925$ to the form $(1 - x_L)^{a(t)}$. The inner error bars indicate the statistical uncertainties and the full bars indicate the quadratic sum of the statistical and systematic uncertainties.*
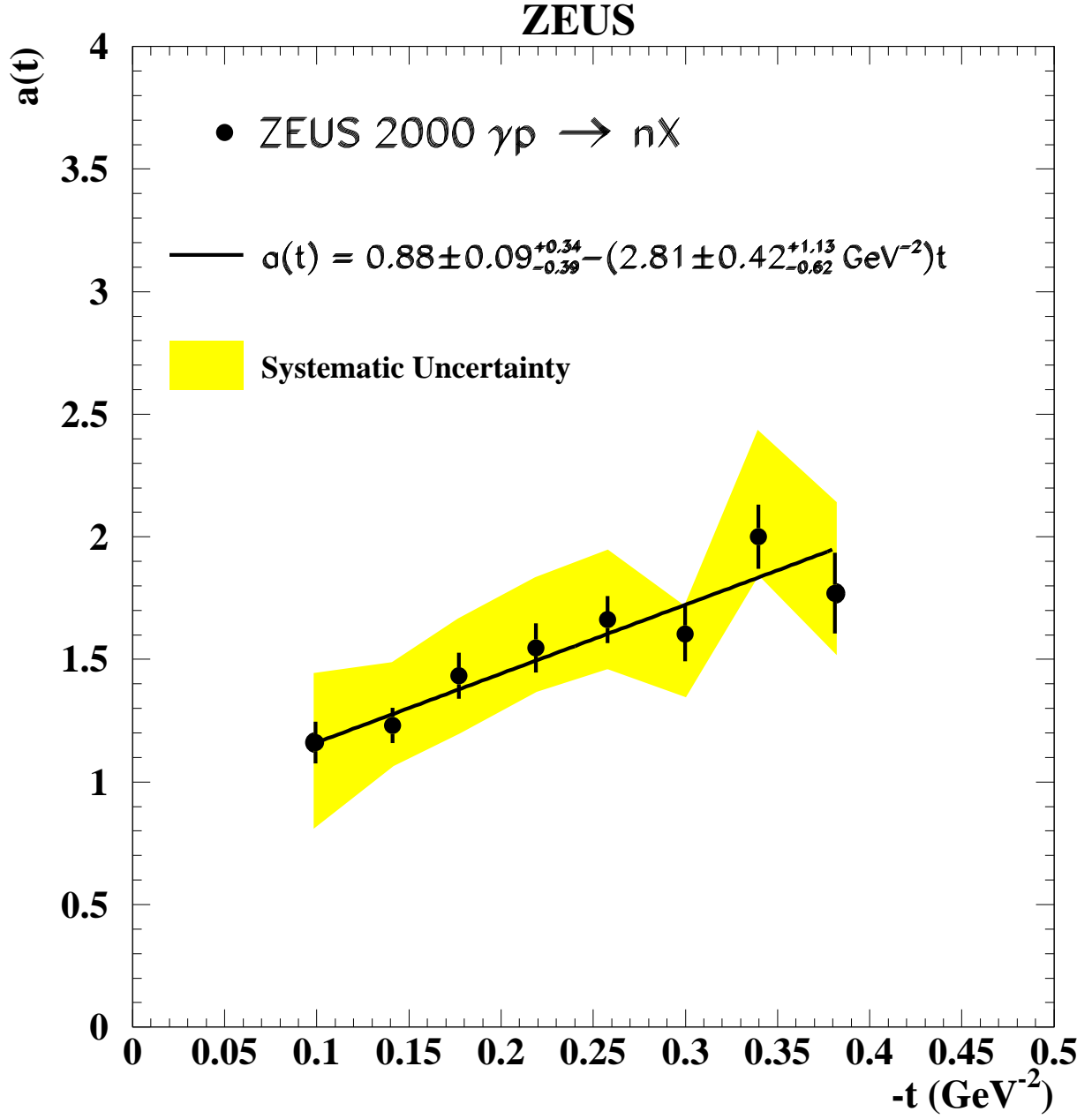
Figure 3: *The powers, $a(t)$, with statistical errors, as a function of $-t$. The solid line is the result of the fit described in the text. The shaded band shows the systematic uncertainty.*